An analytical solution for a low barrier in a turbulent atmosphere

An analytical solution for a low barrier in a turbulent atmosphere

Short title: Analytical solution for low barrier and turbulence

Jens Forssén, Department of Applied Acoustics, Chalmers University of Technology, Göteborg, Sweden

Tel: +46 31 772 2200

E-mail address: jf@ta.chalmers.se

Abstract

The work presented here uses a previously developed substitute sources method (SSM) as the starting point for solving the problem with a low barrier in a turbulent atmosphere. The formulation of the SSM involves a double integral and the numerical solution is computationally demanding. The SSM results are here used as reference. As an intermediate step toward an analytical solution, an expression containing a single integral is found. Its implementation is computationally much less demanding and is here called the fast method. The analytical solution involves further approximations and has a smaller range of validity than the fast method, but could nonetheless be useful. Both the fast method and the analytical solution assume a flat geometry, whereby they can be useful as a complement to scattering cross-section based methods. Moreover, two-dimensional (2-D) modelling is done and no ground surface is considered. Agreement between the SSM and the fast method is reasonably good, and additional restraints are formulated for the applicability of the analytical solution.

PACS: 43.20.Bi, 43.28.Gq, 43.28.Js

1 Introduction

The atmospheric turbulence affects the outdoor sound. Especially in sound shielding situations can the turbulence have a large influence. Here, the main focus is on the sound level increase in a barrier shadow due to the turbulence. One problem of interest is the reduction of traffic noise by the use of buildings or other noise barriers.

In a previous work the results from a scattering cross-section based method were compared with measured data [1]. The turbulence was concluded to give a strong influence at high frequencies or for large geometries. Due to the inherent single-scattering approximation, the method is assumed to be applicable to steep geometries rather than to flat ones. For flat geometries the effects of multiple scattering grows stronger. (A geometry is here seen as flat when the barrier is low in comparison to its distance to the source and to the receiver, so that the diffraction angle is small. Otherwise the geometry is seen as steep.)

The results presented here uses a previously developed substitute sources method (SSM) [2, 3] as starting point. The formulation of the SSM (equation 8) involves a double integral and the numerical solution is computationally demanding; it could be used as a reference method but is too heavy for a fast engineering prediction tool, e.g. for traffic noise mapping. The final result presented here is an analytical solution (equation 26). As an intermediate step an expression (equation 19), containing a single integral, is found, whose numerical implementation could be used as a fast prediction tool. In the following, this numerical implementation is referred to as the *fast method*. The analytical solution involves further approximations and has a smaller range of validity than the fast method, but could nonetheless be useful. Both the fast method and the analytical solution assume a flat geometry, whereby they can be useful as a complement to the scattering cross-section based method discussed above.

The results obtained here are compared with those from the SSM. It could be noted

that the SSM can be applied to any barrier height [3], whereas here, for reduced computation time, the Kirchhoff approximation is used, which makes it applicable to only flat geometries. For the cases without turbulence, the Kirchhoff approximation is assumed to give an error smaller than 1 dB for diffraction angles of about 12° or smaller [2].

For a barrier in a flat geometry, the surface properties of the barrier are of comparably smaller importance than for a barrier in a steep geometry [4]. Therefore the solution for a thin screen presented here can be seen as an approximation for an arbitrary barrier, concerning shape and surface material, in a flat geometry.

It should however be pointed out that for a barrier that is placed on a ground surface, higher order diffraction terms will come into play if the barrier is low compared with the sound wavelength. The field diffracted at the barrier edge and reflected in the ground surface will again be diffracted at the barrier edge and cause a significant additional contribution to the received pressure. This effect is not taken account of in the present paper, where no ground surface is modelled. The effect would give a lower limit to the barrier height, whereas the Kirchhoff approximation gives an upper limit. However, since the turbulence effects generally are of importance at higher frequencies, the results presented here are expected to have a useful range of validity. Within the range of validity, the situation with a ground surface can be approximately modelled as one with four rays, for instance with reduced mutual coherence as done in Ref. [1].

In the present paper only two-dimensional (2-D) modelling is done. Previous studies indicate that 2-D modelling is sufficient for a variety of situations where the increased sound level behind a barrier due to turbulence is sought [3]. The last two questions, about higher order diffraction due to a ground surface and the 2-D modelling, would however benefit from further research.

The next Section describes the theory for the fast method and the analytical solution. In the third Section the numerical results are presented and some examples are plotted. In the Appendix tables display more fully the results for a single screen height

from the SSM and the corresponding errors in the fast method. Section 4 contains the conclusions.

2 Theory

2.1 The Rayleigh integral and the Kirchhoff approximation

In three-dimensional free space the sound pressure $p_{0,3D}$ due to a point source with strength Q can be written

$$p_{0,3D} = Q\frac{\mathrm{e}^{-\mathrm{j}kL}}{L} \tag{1}$$

where k is the wave number, L is the distance, and where the time oscillation $\mathrm{e}^{\mathrm{j}\omega t}$ with the angular frequency ω is omitted. If the point source is extended mathematically along a line parallel with the horizontal z-axis, with L the smallest distance to the receiver, the pressure becomes

$$p_0 = Q\frac{\pi}{\mathrm{j}}\mathrm{H}_0^{(2)}(kL) \tag{2}$$

which can be seen as the corresponding 2-D solution. (The source strength, Q, does however have different units for the point and the line source.) A far field approximation of the Hankel function is used

$$\mathrm{H}_0^{(2)}(x) = \sqrt{\frac{2}{\pi x}}\mathrm{e}^{-\mathrm{j}x+\mathrm{j}\pi/4} \tag{3}$$

which inserted into equation (2) gives the 2-D solution

$$p_0 = Q\sqrt{\frac{2\pi}{kL}}\mathrm{e}^{-\mathrm{j}kL-\mathrm{j}\pi/4}. \tag{4}$$

If the velocity component v_n normal to a flat surface is known, the pressure can be calculated using a Rayleigh integral

$$p = \frac{\omega\rho}{2}\int_\ell v_n \mathrm{H}_0^{(2)}(kR)\mathrm{d}y \tag{5}$$

where ℓ is the line of integration in the vertical y-direction and R is the distance to the receiver from the point y on the line (see Figure 1). (The normal direction is into the halfspace where p is calculated.) It can be noted that the above equations apply to a homogeneous atmosphere. The Rayleigh integral can however be formulated for other cases, for instance for a sound speed profile that models wind or a temperature gradient.

Letting the normal velocity v_n in equation (5) be the free-field velocity on a part of the line ℓ, and zero outside, can be seen as a Kirchhoff approximation for the diffracted field from the corresponding opening. (For a description of the Kirchhoff approximation, see e.g. Ref. [5].) The free field velocity can be found from the free field pressure, p_0, as

$$v_n = \frac{-1}{\mathrm{j}\omega\rho}\nabla p_0 \cdot \mathbf{n} \approx \frac{Q}{\rho c}\frac{d}{R_0}\sqrt{\frac{2\pi}{kR_0}}\mathrm{e}^{-\mathrm{j}kR_0-\mathrm{j}\pi/4} \tag{6}$$

where ρ is the density, R_0 is the distance from the source to where v_n is calculated, d is the projection of R_0 on the normal direction, and where a far-field approximation is used in the last step.

Equation (5) for the received pressure as a Rayleigh integral can now be rewritten as

$$p = Qd_S\int_\ell \frac{\mathrm{e}^{-\mathrm{j}k(R_S+R_R)}}{R_S^{3/2}R_R^{1/2}}\mathrm{d}y = Qd_S\int_\ell \frac{\mathrm{e}^{-\mathrm{j}k(\sqrt{d_S^2+y^2}+\sqrt{d_R^2+y^2})}}{(d_S^2+y^2)^{3/4}(d_R^2+y^2)^{1/4}}\mathrm{d}y \tag{7}$$

where far field approximations are used for both v_n and $\mathrm{H}_0^{(2)}$, as in equations (6) and (3), respectively. In the last step in equation (7) it is assumed that the *substitute surface*, i.e. where the Rayleigh integral is calculated, is at range d_S, where $d_S + d_R = L$ is the total distance to the receiver, and that the source–receiver line is perpendicular to the y-axis. (The notation *substitute surface* is used even though it is a line in 2-D.)

The free field solution p_{free} is taken as when the integration in equation (7) is made over the whole y-axis; $\ell \,\epsilon\, (-\infty, \infty)$, or, equivalently, as twice the result for $\ell \,\epsilon\, (0, \infty)$. In the far field one will approximate the free field, $p_{\text{free}} = p_0$. The screen diffraction solution in the Kirchhoff approximation, p_H, is for integration from the height H of the edge of the screen to infinity; $\ell \,\epsilon\, (H, \infty)$. A solution of p_H can also be found via the integral over the interval of the screen, $\ell \,\epsilon\, (0, H)$, since the result equals $p_{\text{free}}/2 - p_H$. This change of integration domain (sometimes referred to as Babinet's principle, see e.g. Refs. [5, 6]) allows for a fast numerical solution for low screen heights. The power of the received signal is proportional to the square of the absolute value of the pressure amplitude, and here $W = \frac{1}{2}|p|^2$ is simply referred to as the power. The free field power is $W_{\text{free}} = \frac{1}{2}|p_{\text{free}}|^2$ and the diffracted power is $W_H = \frac{1}{2}|p_H|^2$.

2.2 Introduction of turbulence

A change in integration domain is used also for finding the solution including turbulence, as shown below. The estimate of the mean power in the presence of turbulence, $\widetilde{W}$, is found as a double integral over the pressure contribution and its conjugate using a mutual coherence factor (MCF), Γ, which depends on the spatial separation of the points of contribution y_1 and y_2 [7, 2]. Using equation (7) the mean power $\widetilde{W}$ can be written

$$\begin{aligned} \widetilde{W} &= \frac{Q^2 d_S^2}{2} \int_\ell \int_\ell \Gamma(y_1 - y_2) \frac{\mathrm{e}^{-\mathrm{j}k(R_{S1} + R_{R1} - R_{S2} - R_{R2})}}{R_{S1}^{3/2} R_{R1}^{1/2} R_{S2}^{3/2} R_{R2}^{1/2}} \mathrm{d}y_1 \mathrm{d}y_2 \qquad (8) \\ &= \int_\ell \int_\ell \Gamma(y_1 - y_2) D(y_1, y_2) \mathrm{d}y_1 \mathrm{d}y_2 \end{aligned}$$

where $R_{S1} = \sqrt{d_S^2 + y_1^2}$, $R_{R1} = \sqrt{d_R^2 + y_1^2}$, $R_{S2} = \sqrt{d_S^2 + y_2^2}$, $R_{R2} = \sqrt{d_R^2 + y_2^2}$.

A simplifying substitution of variables that is commonly used for expressions like equation (8) is $y_1 + y_2 = 2u$, $y_1 - y_2 = v$ [8, 9]. (See Figure 2.) In these new coordinates Γ depends on v only and some additional symmetry qualities with respect to both u and v can be used.

The next step in the derivation is based on an energy conservation argument. Assume that, for $\ell \,\epsilon\, (-\infty, \infty)$, $\widetilde{W}$ in equation (8) equals W_{free}, i.e. that, in the absence of a screen (and of a ground surface), there is no influence of turbulence on the mean power. The energy conservation assumption can be written

$$W_{\text{free}} = Q^2 d_S^2 \int_{-\infty}^{\infty} \Gamma(v) \int_0^{\infty} \frac{\cos[k(R_{S1} + R_{R1} - R_{S2} - R_{R2})]}{R_{S1}^{3/2} R_{R1}^{1/2} R_{S2}^{3/2} R_{R2}^{1/2}} \mathrm{d}u \mathrm{d}v \qquad (9)$$

where it is taken advantage of that the integrand in equation (9) is a Hermitian function of u, i.e. its real part is even and its imaginary part is odd. When using the energy conservation assumption, the integration domain $u > 0$ (which corresponds to $\frac{1}{2} W_{\text{free}}$) is split up in two parts, $\widetilde{W}_H$ and $\widetilde{W}_C$, so that

$$\widetilde{W}_H + \widetilde{W}_C = \frac{1}{2} W_{\text{free}}. \qquad (10)$$

The integral $\widetilde{W}_H$ is the result when the lines of integration in equation (8) are both (H, ∞), i.e. $\widetilde{W}_H$ is the mean power due to sound propagation above the barrier in a turbulent atmosphere. The remaining integral in $u > 0$ is $\widetilde{W}_C$. (See Figure 2.) The desired result, $\widetilde{W}_H$, is then found by way of finding $\widetilde{W}_C$ and W_{free}, where W_{free} can be obtained from equation (2). Using that the integrand in equation (9) is an even function in v, the integral $\widetilde{W}_C$ can be written

$$\widetilde{W}_C = Q^2 d_S^2 \int_0^{\infty} \Gamma(v) \int_0^{H+v} \frac{\cos[k(R_{S1} + R_{R1} - R_{S2} - R_{R2})]}{R_{S1}^{3/2} R_{R1}^{1/2} R_{S2}^{3/2} R_{R2}^{1/2}} \mathrm{d}u \mathrm{d}v. \qquad (11)$$

It can be shown that the MCF goes toward an asymptotic value when v is increased (see Ref. [9], Eq. 7.65). This value is $\mathrm{e}^{-2\gamma L}$, where γ is the extinction coefficient and L the range of propagation [9], and it is used to rewrite the MCF $\Gamma(v)$ in equation (11) in two terms: a constant term and a term which goes to zero asymptotically, as

$$\Gamma(v) = \mathrm{e}^{-2\gamma L} + \left(1 - \mathrm{e}^{-2\gamma L}\right) \hat{\Gamma}(v) \qquad (12)$$

with

$$\hat{\Gamma}(v) = \frac{\Gamma(v) - \mathrm{e}^{-2\gamma L}}{1 - \mathrm{e}^{-2\gamma L}}. \tag{13}$$

Equation (12) can be seen as causing a separation of the field into a coherent part, corresponding to the factor $\mathrm{e}^{-2\gamma L}$, and an *incoherent* part, corresponding to the factor $1 - \mathrm{e}^{-2\gamma L}$ and having the MCF $\hat{\Gamma}(v)$. To see this, equation (12) can be inserted in equation (8) to calculate $\widetilde{W}_H$:

$$\begin{aligned} \widetilde{W}_H &= \int_H^\infty \int_H^\infty \Gamma\, D \,\mathrm{d}y_1 \mathrm{d}y_2 \qquad (14) \\ &= \mathrm{e}^{-2\gamma L} \int_H^\infty \int_H^\infty D \,\mathrm{d}y_1 \mathrm{d}y_2 + (1 - \mathrm{e}^{-2\gamma L}) \int_H^\infty \int_H^\infty \hat{\Gamma}\, D \,\mathrm{d}y_1 \mathrm{d}y_2. \end{aligned}$$

The first term in the last step of equation (14) is the coherent part and can be found directly from the diffraction solution, without turbulence, as $\mathrm{e}^{-2\gamma L} W_H$.

Using, in equation (11), the rewritten $\Gamma(v)$, as in equation (12), gives

$$\begin{aligned} \widetilde{W}_C = Q^2 d_S^2 \Bigg\{ & \mathrm{e}^{-2\gamma L} \int_0^\infty \int_0^{H+v} \frac{\cos[k(R_{S1} + R_{R1} - R_{S2} - R_{R2})]}{R_{S1}^{3/2} R_{R1}^{1/2} R_{S2}^{3/2} R_{R2}^{1/2}} \mathrm{d}u \mathrm{d}v \qquad (15) \\ & + \left(1 - \mathrm{e}^{-2\gamma L}\right) \int_0^\infty \hat{\Gamma}(v) \int_0^{H+v} \frac{\cos[k(R_{S1} + R_{R1} - R_{S2} - R_{R2})]}{R_{S1}^{3/2} R_{R1}^{1/2} R_{S2}^{3/2} R_{R2}^{1/2}} \mathrm{d}u \mathrm{d}v \Bigg\}. \end{aligned}$$

The first term in the above equation is $\mathrm{e}^{-2\gamma L} W_C$, i.e. $\mathrm{e}^{-2\gamma L}$ times equation (11) with $\Gamma(v) \equiv 1$ (W_C stands for $\widetilde{W}_C$ without turbulence). This term can be rewritten assuming energy conservation for the case without turbulence: $W_C = \frac{1}{2} W_{\text{free}} - W_H$.

Concerning the second term in equation (15), if $\hat{\Gamma}(v)$ goes to zero sufficiently fast, i.e. that $\hat{\Gamma}(v)$ makes the integral contribute only for $v \ll d_S, d_R$, and the screen is low ($H \ll d_S, d_R$), the dominant contribution will be for $y_1,\ y_2 \ll d_S, d_R$. The argument of the cos-function, i.e. the phase difference, can then be approximated using

$$R_{S1} - R_{S2} = \sqrt{d_S^2 + y_1^2} - \sqrt{d_S^2 + y_2^2} \approx \frac{y_1^2 - y_2^2}{2 d_S} = \frac{uv}{d_S} \tag{16}$$

and similarly for $R_{R1} - R_{R2}$. In the denominator of the integrand more crude approximations are used according to

$$d_S^2 + y_1^2 \approx d_S^2, \quad d_S^2 + y_2^2 \approx d_S^2 \tag{17}$$

and similarly for d_R.

Applying the above results to equation (15) gives

$$\widetilde{W}_C = \mathrm{e}^{-2\gamma L}\left(\frac{1}{2}W_{\text{free}} - W_H\right) \tag{18}$$
$$+ \left(1 - \mathrm{e}^{-2\gamma L}\right)\frac{Q^2}{d_S d_R}\int_0^\infty \hat{\Gamma}(v)\int_0^{H+v}\cos\left[kuv\left(\frac{1}{d_S}+\frac{1}{d_R}\right)\right]\mathrm{d}u\mathrm{d}v.$$

The integral with respect to u can be solved analytically. Doing this and writing the solution for $\widetilde{W}_H$ as $\widetilde{W}_H = \frac{1}{2}W_{\text{free}} - \widetilde{W}_C$ (from equation 10) gives

$$\widetilde{W}_H = \mathrm{e}^{-2\gamma L}W_H + \left(1 - \mathrm{e}^{-2\gamma L}\right)\times \tag{19}$$
$$\left\{\frac{1}{2}W_{free} - \frac{Q^2}{k(d_S+d_R)}\int_0^\infty \hat{\Gamma}(v)\sin\left[k(H+v)v\left(\frac{1}{d_S}+\frac{1}{d_R}\right)\right]\frac{\mathrm{d}v}{v}\right\}.$$

The fast method is the numerical implementation of equation (19), the results of which are shown in the following Section.

The different turbulence models used here are described in the next Subsection. For the Kolmogorov model the extinction coefficient is infinite [9], which leads to that equation (19) can be rewritten using $\mathrm{e}^{-2\gamma L} = 0$.

2.3 Turbulence models

The mutual coherence factor (MCF) will in general depend on the choice of turbulence model, its parameter values, the transversal separation, v, the distance of propagation, L, and the sound frequency, f. Here, the starting point is the von Kármán turbulence model with MCF for spherical wave propagation as

$$\Gamma^{\text{vK}}(v) = \exp\left\{-\frac{2L}{K_0 v}\int_0^{K_0 v}\gamma_T\left[1 - \frac{2^{1/6}t^{5/6}}{\Gamma(5/6)}K_{5/6}(t)\right]\right. \tag{20}$$

$$+\gamma_v \left[1 - \frac{2^{1/6} t^{5/6}}{\Gamma(5/6)} \left(K_{5/6}(t) - \frac{t}{2} K_{1/6}(t)\right)\right] \mathrm{d}t \Bigg\}$$

where γ_T and γ_v are the extinction coefficients of the mean field due to temperature and velocity fluctuations, respectively; $K_0 = 2\pi/L_0$, where L_0 is taken as the outer scale of turbulence; $\Gamma(5/6) \approx 1.13$ is the gamma function; and $K_{5/6}$ and $K_{1/6}$ are modified Bessel functions of the second kind. The total extinction coefficient can be written

$$\gamma = \gamma_T + \gamma_v = \frac{3}{10} \pi^2 A k^2 K_0^{-5/3} \left(\frac{C_T^2}{T_0^2} + \frac{4 C_v^2}{c_0^2}\right) \tag{21}$$

where $A \approx 0.0330$, T_0 is the mean temperature, c_0 is the mean sound speed, and C_T^2 and C_v^2 are the structure parameters describing the strengths of temperature and velocity fluctuations, respectively. (For the above formulation of Γ^{vK} Ref. [9] was used.)

It is assumed that the MCF for spherical wave propagation can be used for the 2-D situations studied here without significant errors in the calculated barrier insertion loss. A previous comparison, involving a Kolmogorov turbulence model, indicates that such 2-D modelling is sufficient [3].

In the region where the Kirchhoff approximation is valid, it is reasonable to assume that, in the MCF in equations (20) and (19), the longitudinal distance $L = d_S + d_R$ could be used as a good approximation. In a more strict approach, the turbulence is introduced first after the screen, giving $L = d_R$, which is used in the numerical tests made here.

The range of test calculations used here provides a good opportunity to compare different turbulence models. Here the Gaussian and the Kolmogorov models are studied in addition to the von Kármán model. The models are connected according to Ostashev [9], where the von Kármán spectrum is assumed to be the model spectrum of turbulence. Following the same reference, it is then assumed that, for the Gaussian and the von Kármán spectra, the integral length scales are the same for the normalised longitudinal correlation functions of the velocity fluctuations, and that the same is true

for the temperature fluctuations. It is also assumed that the variances of the turbulent fields are the same. The resulting MCF for the Gaussian model can then be written

$$\Gamma^{\mathrm{G}}(v) = \exp\left[-2\gamma_T L\left(1 - \frac{\Phi(v/l)}{v/l}\right) - 2\gamma_v L\left(1 - \frac{1}{2}\frac{\Phi(v/l)}{v/l} - \frac{1}{2}\mathrm{e}^{-v^2/l^2}\right)\right] \quad (22)$$

where $\Phi(v/l) = \int_0^{v/l} \mathrm{e}^{-s^2}\mathrm{d}s$ and $l = \frac{2\Gamma(5/6)}{\Gamma(1/3)}K_0^{-1} \approx 0.843K_0^{-1}$. By connecting the Gaussian and the von Kármán spectra in this way, the Gaussian spectrum can be seen as modelling the larger scales of the turbulence. It should be noted that, for other values of the strength and the correlation length, l, the Gaussian spectrum can model a different range of scales.

The Kolmogorov spectrum is seen as an approximation for the smaller scales, within the inertial range, and the MCF can be written

$$\Gamma^{\mathrm{K}}(v) = \exp\left[-\frac{3}{8}B\left(\frac{C_T^2}{T_0^2} + \frac{22}{3}\frac{C_v^2}{c_0^2}\right)k^2 v^{5/3}L\right] \quad (23)$$

where $B \approx 0.364$.

2.4 The analytical solution

In the limit of small screen heights, the effect of turbulence is assumed to be dominated by the larger scales. This is due to that the larger scales scatter in directions more near forward, which can be seen from a Bragg scattering analogy (e.g. [1]). For the largest scales the von Kármán turbulence model is well approximated by the Gaussian one as it is used here, and hence the Gaussian model could be used in equation (19) to find an approximation for near zero screen heights. (It could be noted that one should be able to reach the same end result by using the von Kármán model, but the Gaussian model provides a simpler analysis.)

For this approximation, $\hat{\Gamma}(v)$ in equation (19) is replaced by a small argument approximation of equation (22). For $v \ll l$ one can find that equation (22) can be approximated as

$$\Gamma^{\mathrm{G}}(v) = \exp\left(-\alpha v^2\right) \tag{24}$$

with $\alpha = (\gamma_T + 2\gamma_v)2L/(3l^2)$. (For different length scales of the temperature and the velocity fluctuations, l_T and l_v respectively, one can write $\alpha = 2\gamma_T L/(3l_T^2) + 4\gamma_v L/(3l_v^2)$.) If strong turbulence effects are assumed, $\hat{\Gamma}(v)$ will go to zero fast enough to make the integrand in equation (19) contribute only for small arguments of the sin-function, and an approximation as $\sin(x) \approx x$ can be used, assuming $|x| \ll 2\pi$. With the latter approximation and $\hat{\Gamma}(v) = \exp\left(-\alpha v^2\right)$, equation (19) can be rewritten as

$$\widetilde{W}_H = \mathrm{e}^{-2\gamma L} W_H + \left(1 - \mathrm{e}^{-2\gamma L}\right) \left[\frac{1}{2} W_{free} - \frac{Q^2}{d_S d_R} \int_0^\infty (H + v) \mathrm{e}^{-\alpha v^2} \, \mathrm{d}v\right]. \tag{25}$$

The integral is solved to give the analytical solution

$$\widetilde{W}_H = \mathrm{e}^{-2\gamma L} W_H + \left(1 - \mathrm{e}^{-2\gamma L}\right) \left[\frac{1}{2} W_{free} - \frac{Q^2}{2 d_S d_R} \left(H \sqrt{\frac{\pi}{\alpha}} + \frac{1}{\alpha}\right)\right]. \tag{26}$$

The restriction for the small argument approximation of the sin-function used above can be written as

$$\left| k(H + v) v \left(\frac{1}{d_S} + \frac{1}{d_R}\right) \right| \ll 2\pi \tag{27}$$

where all variables are positive except H which may be positive or negative. The inequality (27) should hold as long as αv^2 in equation (25) is near 1 or smaller, where $\alpha v^2 = 1$ is attained at the correlation radius $v = v_c$. If the term corresponding to H in equation (27) is taken to separately fulfil the inequality, and $v = v_c$ is used, a limit on H can be written as $k|H| v_c \, (1/d_S + 1/d_R) \ll 2\pi$. If the other term is restricted in the same way, the result can be written as $k v_c^2 \, (1/d_S + 1/d_R) \ll 2\pi$. This can be formulated in terms of the first Fresnel zone, v_{F}, which here is given by $v_{\mathrm{F}}^2 = 2\pi/[k(1/d_S + 1/d_R)]$, assuming $kd_S, kd_R \gg 1$. As a result, the two inequalities to be fulfilled are $|H| v_c \ll v_{\mathrm{F}}^2$ and $v_c^2 \ll v_{\mathrm{F}}^2$.

3 Numerical test

In the numerical tests the fast method is evaluated using the substitute sources method (SSM) as reference. The fast method is implemented from equation (19) and the SSM from equation (8). Results for different turbulence models are studied but the main results are for the von Kármán model. Thereafter follows an evaluation of the analytical solution, equation (26).

The consequences of changing the integration area, equation (10), and the low angle approximations, as in equations (16) and (17), applied in the above derivation, are not easily foreseen. The calculations therefore constitute a parameter study with aim to investigate the limits of applicability of both the fast method and the analytical solution, as well as to study the behaviour of the physical problem in itself.

The test calculations are made for a single source–receiver distance $L = d_S + d_R$, with source–barrier distance $d_S = 100$ and barrier–receiver distance $d_R = 900$ m, but for different frequencies, screen heights and turbulence parameters. Only velocity fluctuations are considered ($C_T^2 = 0$), with strengths $C_v^2 = 10^{-4}$, 10^{-3}, 10^{-2}, 10^{-1}, 1, and $10\,\mathrm{m}^{4/3}\mathrm{s}^{-2}$, and with $L_0 = 2\pi/K_0 = 1,\ 10,\ 10^2$, and 10^3 m. The frequencies are $f = 63$, 125, 250, 500, and 1000 Hz. Some of the values chosen for the parameters correspond to unrealistic situations, mainly concerning the strong turbulence. Scaling properties can however be applied, as will be described below, which change the range of realistic values. The large values of d_S and d_R are chosen to give substantial influence of moderately strong turbulence at frequencies of interest for traffic noise. That the distances d_S and d_R differ by a large factor fits well to the SSM, where the turbulence is modelled on only one side of the barrier, and it also fits to many noise barrier situations, where the barrier is located relatively close to the source or to the receiver (the reciprocal problem).

The different combinations of the values of f, L_0, and C_v^2 give 120 cases, of which a few results are shown below as examples of trends and special behaviour. A more extensive collection of results are tabulated in the Appendix. For each case the screen

height is varied with fine discretisation over a large range. The plots show the increased sound pressure level due to the turbulence, $\Delta L_p = 10\log_{10}(\widetilde{W}_H/W_H)$, as a function of screen height, for $H\epsilon(-10, 30)$ m. A negative screen height thus stands for a screen edge that is below the line of sight. At $H = 20$ m the diffraction angle will be about 12°, which is assumed to give less than 1 dB error due to the Kirchhoff approximation. For the value of the sound speed $c_0 = 340$ m/s is used.

Results for other source–receiver distances than $L = 1000$ m can be found from using scaling properties of the sound field and of the MCF. To demonstrate this, assume that one wants results for a geometry scaled by a factor s. For instance for $s = 0.1$ the values of the geometrical parameters d_S, d_R and H are reduced to one tenth of their original value. Without turbulence the result for the scaled geometry is found from the result for the original geometry at ten times the frequency (i.e. divided by s). For a turbulent atmosphere the parameters of the MCF that involve geometry or frequency are scaled accordingly: L_0 is multiplied by s (i.e. K_0 is divided by s), L is multiplied by s, and k is divided by s. Finally, it can be found that by multiplying C_v^2 by $s^{-2/3}$, the MCF is kept the same in the scaled parameters. For example, with $s = 0.1$, $[d_S,\, d_R,\, H,\, f,\, L_0,\, C_v^2] = [100,\, 900,\, 10,\, 100,\, 10,\, 1]$ gives the same received pressure level relative to free field as $[d_S,\, d_R,\, H,\, f,\, L_0,\, C_v^2] = [10,\, 90,\, 1,\, 1000,\, 1,\, 4.64]$, where $0.1^{-2/3} \approx 4.64$. (The units of the parameters are [m, m, m, Hz, m, $\mathrm{m}^{4/3}\mathrm{s}^{-2}$], and are left out in the following.)

In Figures 4–12 the three thicker curves show the reference results from the SSM, using the von Kármán, Kolmogorov, and Gaussian models. The three thinner curves show the fast method results for the same turbulence models. The analytical solution is exemplified in Figures 8 and 11. (Line styles are plotted in Figure 3.)

3.1 Results using the von Kármán model

Concerning general trends in the SSM results, the 120 cases with the von Kármán model show a larger turbulence influence, ΔL_p, when f, L_0, or C_v^2 increases. The de-

pendence on L_0 can be explained by that an increase in L_0, while keeping C_v^2 constant, exclusively adds to the strength of the large scale turbulence. For a larger part of these cases, the results from the fast method follow the SSM results well.

In the Appendix tables of the SSM results and the corresponding errors when using the fast method are shown for the screen height $H = 20$ m. Most results show good agreement, but larger errors (more than 1 dB at $H = 20$ m) do appear when L_0 and the correlation radius, v_c, are large at the same time. The correlation radius grows large when C_v^2 or f becomes sufficiently small. Probably large angle scattering is important here, i.e. the low angle approximation is the cause for the errors: L_0 does not fulfil $L_0 \ll d_S,\, d_R$ at the same time as the corresponding large scale turbulence dominates the scattering. Here, this takes place for $L_0 = 10^2$ or 10^3 and when the correlation radius no longer fulfils $v_c \ll d_S,\, d_R$. (These cases are marked by an asterisk, *, in the Appendix, using $v_c \leq d_S/10$ as a limiting condition. For these results the correlation radius is found numerically from equation 20.) An example of these deviations is shown in Figure 4, where $v_c = 23$ m and $[f,\, L_0,\, C_v^2] = [1000,\, 10^2,\, 10^{-2}]$.

As can be seen in the Appendix, large errors can be found in other cases than with large L_0 and v_c, as discussed above. Of these cases, the ones with error larger than 1 dB at $H = 20$ m are underlined. The error is 2 dB at most.

3.2 Other results

Concerning the results for the Gaussian and Kolmogorov turbulence models, some larger deviations than for the von Kármán model can be found, as for instance in Figures 6, 9, and 10.

In Figures 7, 8, and 10 it can be seen how the Gaussian and Kolmogorov models relate to the von Kármán model. In Figure 8 the Gaussian and the von Kármán results match, whereas in Figure 10 it is instead the Kolmogorov and the von Kármán results that match. This relates to the correlation radius, or to the value of γL, where a small value of γL gives a large correlation radius. Here $\gamma L = \gamma_v d_R = 0.05$ for the results in

Figure 8 and $\gamma_v d_R = 105$ for those in Figure 10. When γL is small, and the correlation radius is large, the large scales become influential, which are well approximated by the Gaussian model as it is used here. In the opposite case, with γL large, and a small correlation radius, the smaller scales are the most influential, for which the Kolmogorov model is a good approximation. The conclusion is made in Ref. [10] that for $\gamma L < 0.5$ and $\gamma L \geq 100$ the Gaussian and the Kolmogorov model, respectively, gives a good approximation of the MCF, which is in accordance with the results in Figures 8 and 10. However, the variation of the screen height adds to the complexity. For example, the results in Figure 7, for which $\gamma_v d_R = 0.56$, show how the von Kármán results first match the Gaussian ones for the smaller screen heights and then tend to the Kolmogorov results for the larger screen heights. This follows the Bragg scattering analogy, in which the smaller scales cause the scattering at large angles, i.e. for larger screen heights.

It should be noted that in some cases where the SSM predicts a ΔL_p of around 5 dB or smaller, the fast method with the Kolmogorov model gives very large errors, as exemplified in Figure 12. The reason for this is not clear but may be due to the infinite turbulence strength given by the Kolmogorov model in the limit of large scales. Moreover, some cases with the Kolmogorov model, both for the fast method and for the SSM, show oscillations in the results for larger screen heights, which are assumed to be due to numerical problems. It should also be noted that in the derivation of a MCF for a turbulent atmosphere $kv_c \gg 1$ is assumed [9]. Here, $kv_c > 10$ is fulfilled for all cases with the von Kármán model, except for the two cases $[f,\, L_0,\, C_v^2] = [1000,\, 10^2,\, 10]$ and $[1000,\, 10^3,\, 10]$, where $kv_c \approx 3$.

Concerning the analytical solution, the results therefrom follow well the SSM results with the von Kármán model for all cases where the fast method is shown to work and under the additional restraints $v_c^2 \ll v_\mathrm{F}^2$ and $|H|v_c \ll v_\mathrm{F}^2$, as described above. In Figures 8 and 11 two examples are shown, where the von Kármán results match the Gaussian and the Kolmogorov ones, respectively. The restraints for these cases are given by $v_c^2/v_\mathrm{F}^2 = 0.009$ and $v_\mathrm{F}^2/v_c = 60$ m for Figure 8, and $v_c^2/v_\mathrm{F}^2 = 0.004$

and $v_{\mathrm{F}}^2/v_c = 90$ m for Figure 11. That one has $v_c^2/v_{\mathrm{F}}^2 \ll 1$ says that the additional approximations for the analytical solution are valid when $H \ll 60$ and 90 m, respectively. Summarising the numerical tests, the additional restraints for when the analytical solution can be used with small errors can be formulated as $v_c^2/v_{\mathrm{F}}^2 < 0.1$ and $|H| < 0.1 v_{\mathrm{F}}^2/v_c$.

The computation times for the different methods have been evaluated on a contemporary desktop computer for single cases with the von Kármán turbulence model and for the highest sound frequency (e.g. for the results shown in Figures 4 and 8–12). The computation time was about half an hour for the reference method, the SSM, and about ten seconds for the fast method. The implementation of the analytical solution provided at least a hundred times faster calculations than the fast method.

4 Discussion and conclusions

The problem with a low noise-barrier in a turbulent atmosphere, without the influence of a ground surface, has been studied analytically and numerically in two-dimensional space. The study uses a previously developed substitute sources method (SSM) [2, 3] as starting point. The formulation of the SSM (equation 8) involves a double integral and the numerical solution is computationally demanding; it is here used as a reference method but is too heavy for a fast engineering prediction tool. The final result is an analytical solution (equation 26). As an intermediate step an expression (equation 19), containing a single integral, is found, whose numerical implementation can be used as a fast prediction tool, here called the fast method.

The analytical solution involves further approximations and has a smaller range of validity than the fast method, but could nonetheless be useful. Both the fast method and the analytical solution assume a flat geometry, whereby they can be useful as a complement to scattering cross-section based methods which are assumed to be best applicable to steeper geometries.

For application of the fast method or the analytical solution to a situation including

a ground surface, the barrier must be tall in comparison with the wavelength, since higher order diffraction contributions are not modelled. At the same time the barrier must be low enough, also without a ground surface, to give small diffraction angles (about $12°$ or smaller).

Test calculations in the form of parameter studies have been used to evaluate the fast method and the analytical solution with the SSM as reference. A reasonably good over-all agreement was shown and the errors are concluded to mainly be due to the low-angle approximations, and additional restraints were formulated for the analytical solution. Moreover, scaling properties were described, which increase the range of the parameter study.

Effects of using different turbulence models have been studied, both in the fast method and in the SSM. Examples were found where the results from the von Kármán model were either followed by the ones from the Gaussian model or by the ones from the Kolmogorov model.

Appendix A

The Tables below show, for a single screen height $H = 20$ m, the increase in sound pressure level due to the turbulence, ΔL_p, calculated using the SSM, and the corresponding errors of the fast method.

The results marked by an asterisk (*) are for cases where both the outer scale, L_0, and the correlation radius, v_c, are large, i.e. no longer fulfil $L_0,\, v_c \ll d_S,\, d_R$, where $d_S = 100$ m is the source–screen distance and $d_R = 900$ m the screen–receiver distance. The asterisk marks cases with v_c larger than 10 m and with $L_0 = 10^2$ or 10^3 m, for which it is assumed that the low angle approximations are no longer applicable, and large errors are possible.

Large errors are found in other cases than those marked by asterisks. The errors are between 1 and 2 dB, and the results are underlined.

	$C_v^2 = 10^{-4}$	10^{-3}	10^{-2}	10^{-1}	1	10
f =63	0.0	0.0	0.0	0.0	0.0	0.1
125	0.0	0.0	0.0	0.0	0.1	0.7
250	0.0	0.0	0.0	0.1	0.7	4.2
500	0.0	0.0	0.1	0.6	3.7	11.2
1000	0.0	0.0	0.3	2.6	9.6	18.0

Table B1. ΔL_p for cases with $L_0 = 1$ m.

	$C_v^2 = 10^{-4}$	10^{-3}	10^{-2}	10^{-1}	1	10
f =63	0.0	0.0	0.0	0.0	0.0	0.2
125	0.0	0.0	0.0	0.0	0.1	0.8
250	0.0	0.0	0.0	0.1	0.5	1.7
500	0.0	0.0	0.0	0.2	0.8	1.4
1000	0.0	0.0	0.1	0.3	0.7	1.0

Table B2. Error of the fast method corresponding to the results in table B1.

	$C_v^2 = 10^{-4}$	10^{-3}	10^{-2}	10^{-1}	1	10
f =63	0.0	0.0	0.0	0.0	0.5	3.1
125	0.0	0.0	0.0	0.3	2.0	7.9
250	0.0	0.0	0.1	0.9	5.2	12.9
500	0.0	0.0	0.3	2.3	9.2	17.4
1000	0.0	0.1	0.7	4.6	13.5	21.2

Table B3. ΔL_p for cases with $L_0 = 10$ m.

	$C_v^2 = 10^{-4}$	10^{-3}	10^{-2}	10^{-1}	1	10
f =63	0.0	0.0	0.0	0.0	0.3	1.3
125	0.0	0.0	0.0	0.0	0.3	0.7
250	0.0	0.0	0.0	0.1	0.4	0.6
500	0.0	0.0	0.1	0.4	0.5	0.6
1000	0.0	0.0	0.2	0.7	0.4	0.7

Table B4. Error of the fast method corresponding to the results in table B3.

	$C_v^2 = 10^{-4}$	10^{-3}	10^{-2}	10^{-1}	1	10
f =63	0.0⋆	0.0⋆	0.0⋆	0.2⋆	2.0⋆	7.6
125	0.0⋆	0.0⋆	0.1⋆	0.5⋆	3.7 ⋆	11.1
250	0.0⋆	0.0⋆	0.3⋆	2.6⋆	10.5	18.3
500	0.0⋆	0.0⋆	0.3⋆	2.6	10.5	18.3
1000	0.0⋆	0.1⋆	0.8⋆	4.9	14.8	21.6

Table B5. ΔL_p for cases with $L_0 = 10^2$ m.

	$C_v^2 = 10^{-4}$	10^{-3}	10^{-2}	10^{-1}	1	10
f =63	0.0⋆	0.0⋆	0.0⋆	0.2⋆	0.9⋆	0.7
125	0.0⋆	0.0⋆	0.1⋆	0.8⋆	1.3⋆	0.3
250	0.0⋆	0.1⋆	0.5⋆	1.9⋆	0.9	0.4
500	0.0⋆	0.2⋆	1.4⋆	2.0	0.5	0.6
1000	0.1⋆	0.8⋆	2.5⋆	1.4	0.2	0.8

Table B6. Error of the fast method corresponding to the results in table B5.

	$C_v^2 = 10^{-4}$	10^{-3}	10^{-2}	10^{-1}	1	10
f =63	0.0⋆	0.0⋆	0.0⋆	0.3⋆	2.6⋆	8.7
125	0.0⋆	0.0⋆	0.1⋆	0.6⋆	4.2	11.8
250	0.0⋆	0.0⋆	0.1⋆	1.3⋆	7.4	15.2
500	0.0⋆	0.0⋆	0.3⋆	2.7	11.2	18.5
1000	0.0⋆	0.1⋆	0.8⋆	5.0	15.2	21.7

Table B7. ΔL_p for cases with $L_0 = 10^3$ m.

	$C_v^2 = 10^{-4}$	10^{-3}	10^{-2}	10^{-1}	1	10
f =63	0.0⋆	0.1⋆	0.9⋆	2.1⋆	1.3⋆	0.6
125	0.1⋆	0.5⋆	2.1⋆	2.4⋆	1.2	0.3
250	0.2⋆	1.5⋆	2.7⋆	2.4⋆	0.7	0.5
500	0.9⋆	2.8⋆	2.9⋆	2.0	0.4	0.6
1000	2.3⋆	3.1⋆	2.7⋆	1.4	0.2	0.8

Table B8. Error of the fast method corresponding to the results in table B7.

References

[1] Forssén J. and Ögren, M. Barrier noise-reduction in the presence of atmospheric turbulence: Measurements and numerical modelling. Applied Acoustics, Vol. 63, 2002, pp. 173-187.

[2] Forssén, J. Calculation of noise barrier performance in a turbulent atmosphere by using substitute sources above the barrier. Acustica, Vol. 86, 2000, pp. 269-275.

[3] Forssén J. Calculation of noise barrier performance in a three-dimensional turbulent atmosphere using the substitute-sources method. Acustica–Acta Acustica, Vol. 88, 2002, pp. 181-189.

[4] L'Esprance, A., Nicolas, J. and Daigle, G. A. Insertion loss of absorbent barriers on ground. J. Acoust. Soc. Am., Vol. 86, 1989, pp. 1060-1064.

[5] Pierce, A. D. Acoustics: an introduction to its physical principles and applications. Acoustical Society of America, Woodbury, N.Y., 1989.

[6] Barton, G. Elements of Green's functions and propagation: potentials, diffusion, and waves. Clarendon Press, Oxford, 1989.

[7] Salomons, E. M. A coherent line source in a turbulent atmosphere. J. Acoust. Soc. Am., Vol. 105, 1999, pp. 652-657.

[8] Ishimaru, A. Wave propagation and scattering in random media. IEEE Press (and Oxford University Press, Oxford), New York, 1997.

[9] Ostashev V. E. Acoustics in moving inhomogeneous media. E & FN Spon (an imprint of Thomson Professional), London, 1997.

[10] Ostashev, V. E., Brähler, B., Mellert, V. and Goedecke, G. H. Coherence functions of plane and spherical waves in a turbulent medium with the von Karman spectrum of medium inhomogeneities. J. Acoust. Soc. Am., Vol. 104, 1998, pp. 727-737.

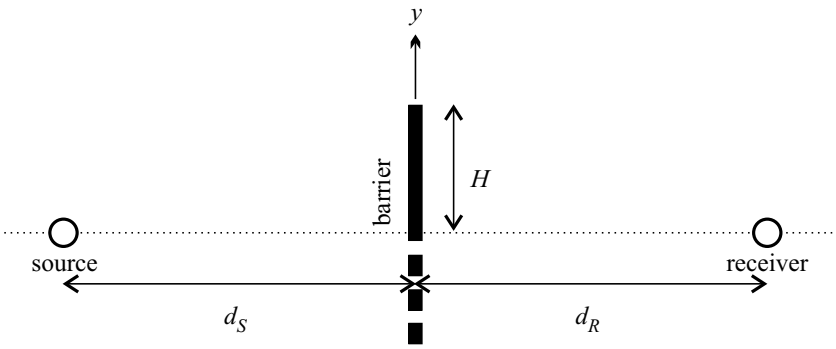

Figure 1: Geometrical situation with source, barrier and receiver.

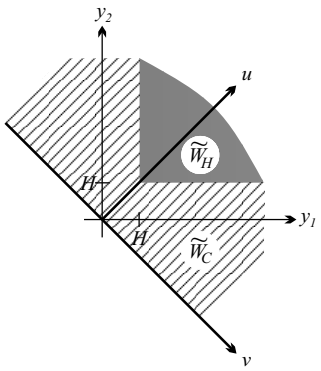

Figure 2: Integration domains for $u > 0$. The domain $\widetilde{W}_H$ is shown in grey and the domain $\widetilde{W}_C$ is striped.

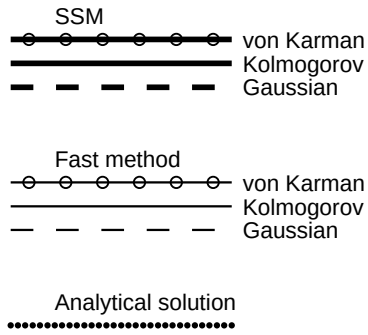

Figure 3: Legend for plotted results in Figures 4–12.

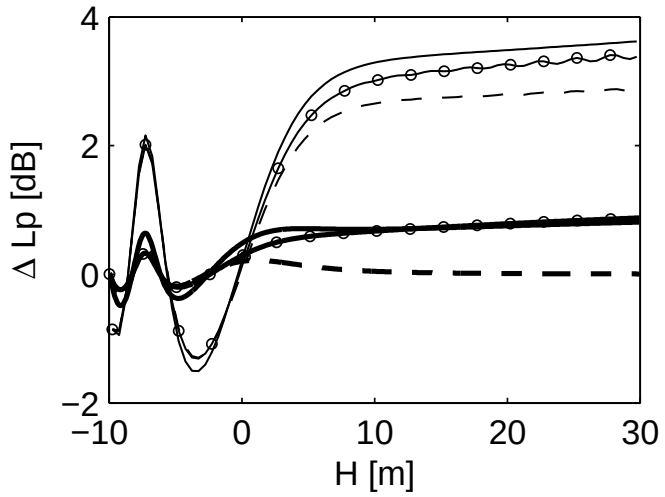

Figure 4: Results for $[f,\, L_0,\, C_v^2] = [1000,\, 100,\, 0.01]$. (The units [Hz, m, $\mathrm{m}^{4/3}\mathrm{s}^{-2}$] are omitted in the following.)

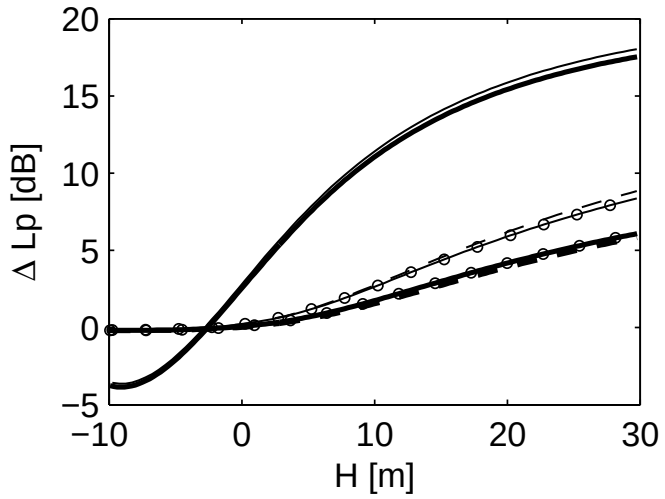

Figure 5: Results for $[f,\ L_0,\ C_v^2] = [250,\ 1,\ 10]$.

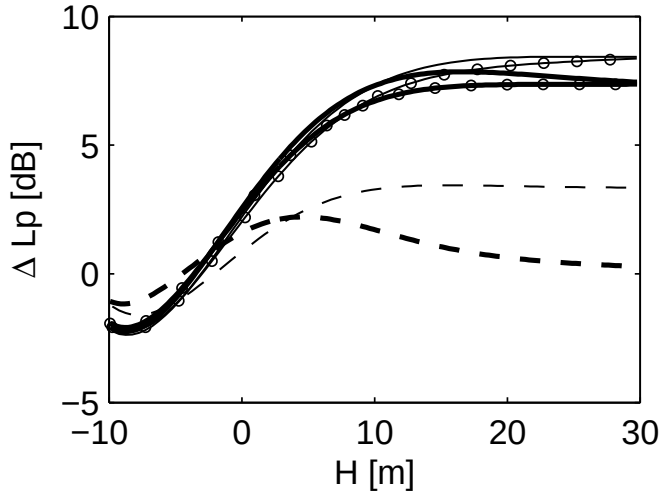

Figure 6: Results for $[f,\ L_0,\ C_v^2] = [250,\ 1000,\ 1]$.

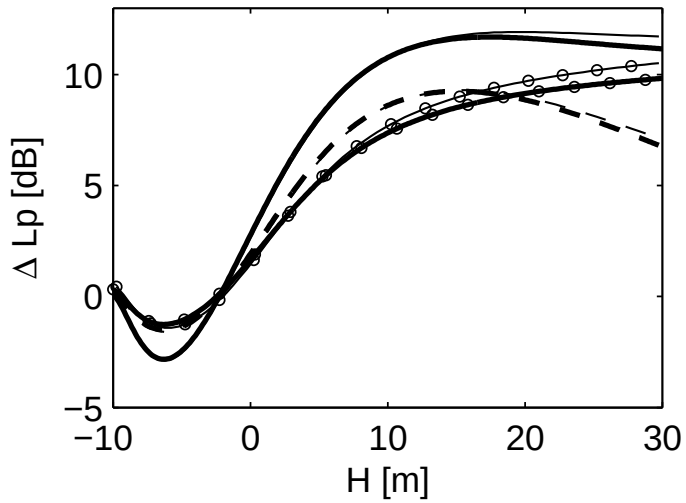

Figure 7: Results for $[f,\ L_0,\ C_v^2] = [500,\ 10,\ 1]$.

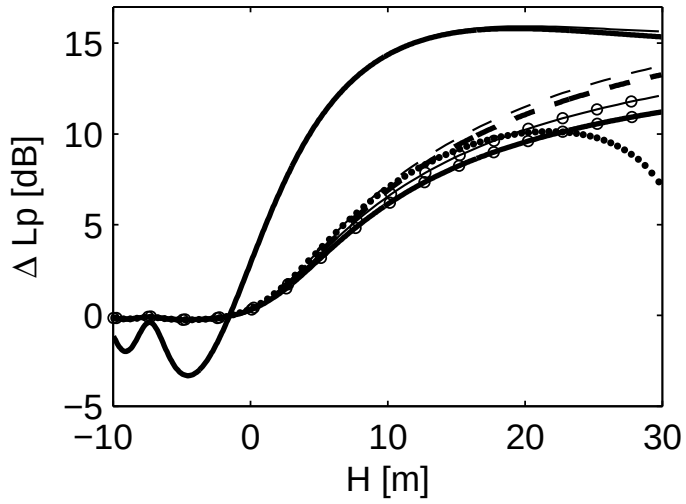

Figure 8: Results for $[f,\ L_0,\ C_v^2] = [1000,\ 1,\ 1]$.

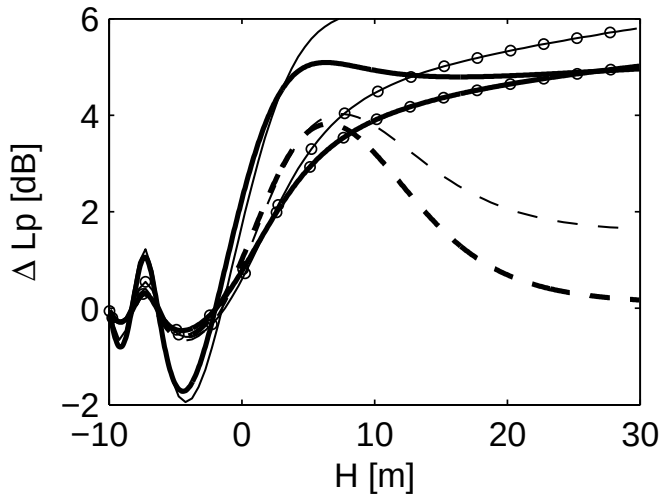

Figure 9: Results for $[f,\ L_0,\ C_v^2] = [1000,\ 10,\ 0.1]$.

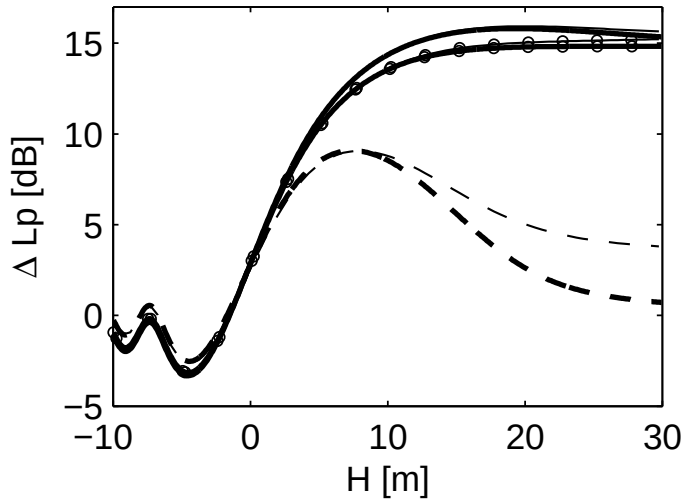

Figure 10: Results for $[f,\ L_0,\ C_v^2] = [1000,\ 100,\ 1]$.

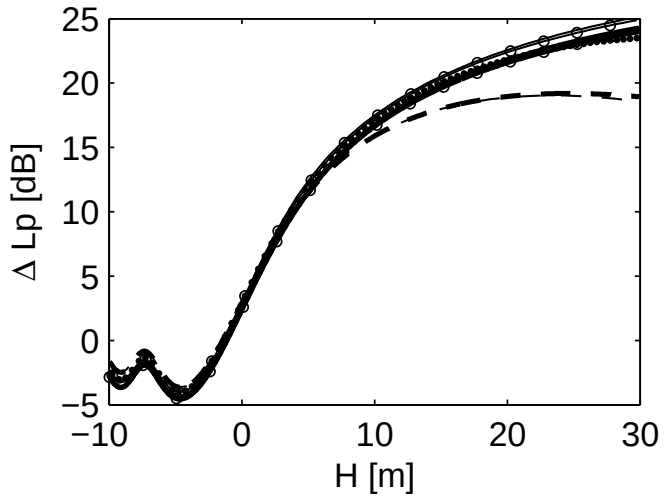

Figure 11: Results for $[f,\, L_0,\, C_v^2] = [1000,\, 100,\, 10]$.

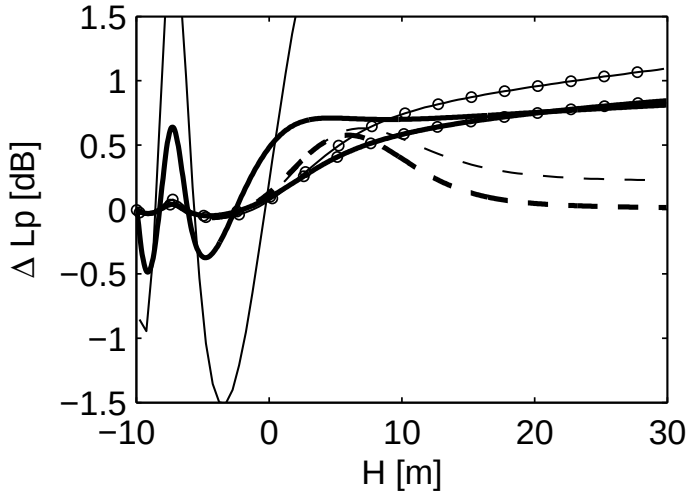

Figure 12: Results for $[f,\, L_0,\, C_v^2] = [1000,\, 10,\, 0.01]$.